A PARAMETRIC STUDY OF PART DISTORTIONS IN FDM USING 3D FEA

Yizhuo Zhang and Y. Kevin Chou
Mechanical Engineering Department, The University of Alabama, Tuscaloosa, AL 35487

Abstract

We developed a finite element model to simulate the fused deposition modeling (FDM) process. The model considers the coupled thermal and mechanical analysis and incorporates the element activation function to mimic the additive nature of FDM. Due to repetitive heating and cooling in the FDM process, residual stresses accumulate inside the part during the deposition. The model is also used to evaluate the part distortions, revealing distortion features such as vaulting shapes and distortion-core shifting. A parametric study, three factors and three levels, was performed to evaluate the effects of the deposition parameters on residual stresses and part distortions. Prototype models with larger sizes were fabricated, measured, and compared with the simulations.

The simulation results show that (1) the scan speed is the most significant factor to part distortions, followed by the layer thickness, (2) the road width alone is insignificant, however, the interaction between the road width and the layer thickness is significant too, and (3) there are other two-way and three-way interactions that are of secondary significance. Residual stresses increase with the layer thickness, and increase with the road width, to a less extent though, yet largely affected by the layer thickness. The FDM part distortions from the experiment show a similar trend as in the simulations, but no quantitative correlation.

Introduction

FDM is one of widely used solid freeform fabrication (SFF) systems because of the inexpensive machinery and durable part materials. In FDM, the thermoplastic material is heated to a semi-molten state and then extruded as an ultra-thin filament. While the extrusion nozzle is moving according to the toolpath defined by the part cross-sectional boundary, the material is deposited atop the previous layer and heat dissipation by conduction and forced convection causes the material to quickly solidify with the surrounding filaments. The bonding between filaments encompasses the local re-melting of the previously solidified material and diffusion [1]. Part geometry in SFF has been a frequently studied topic. Recently, Mahesh et al. used a benchmark part to evaluate several SFF processes and the measured tolerances such as flatness and symmetry were compared [2]. The authors noted that the residual-stress induced distortions (e.g. warpage and delamination) are prominent. As other SFF processes, in FDM, the heating and rapid cooling cycles of the work materials will aggravate non-uniform thermal gradients and cause stress build-up that consequently results in part distortions. Qiu et al. studied the toolpath effects in FDM and proposed an algorithm to match the toolpath with the extrusion speed so to eliminate voids and to correct overfill and underfill defects [3]. Pennington et al. conducted an experimental study to investigate factors significant to dimensional accuracy in FDM. The authors reported that the part size, the location and the envelope temperature have dominant effects [4]. Jiang and Gu also studied the extrusion phenomenon in FDM and reported that process parameters are critical to the part accuracy [5].

Most of SFF processes involve localized energy transport, mass transfer, phase changes, and thermally-induced mechanical loading. Due to high process temperatures, repetitive thermal cycles, and continuous geometric changes, process modeling and simulations of SFF are challenging. Numerical approaches have been applied to model residual stresses in SFF processes. Dalgarno et al. conducted structural analyses to model the part curling development in the selective laser sintering (SLS) process [6]. It was reported that double sintering the first two layers to relieve the strains would significantly reduce the curling level. Sonmez and Hahn developed thermomechanical models for the laminated object manufacturing (LOM) process, correlating process parameters with temperature and stress distributions in the laminate during fabrications, and further suggested that a large roller diameter and a slower roller speed are favorable for bonding [7]. Chin et al. extended an earlier 1-D model to establish thermomechanical models of layers, droplet columns and adjacent droplets in the shape deposition manufacturing (SDM) process [8]. While the localized substrate preheating method was proved ineffective, process-induced preheating seemed to be effective in the reductions of thermal gradients and residual stresses. Nickel et al. developed a 3-D finite element analysis (FEA) model to study the effect of the deposition pattern on the resulting stresses and deflections in SDM [9]. It was suggested that a raster pattern with the primary laser moving direction normal to the part major axis produces the least deflections.

A few references can be found regarding to the FEA studies of part distortions in liquid-based SFF processes. Wiedemann et al. developed methods to evaluate photopolymers with respect to the dynamics of polymerization and shrinkage, also the sensitivity of polymerization to process conditions [10]. A numerical simulation of part distortions was applied to reveal the interaction between the material properties and the process parameters. The time dependent shrinkage and build-up of strength during the polymerization were investigated. It was concluded that the build process must be optimized to reduce internal stresses in SLA. Bugeda et al. modeled the mechanical aspect in stereolithographic apparatus (SLA) to study the influence of different constructive and numerical parameters in the curl distortion caused by resin shrinkage [11]. The curl distortion was found to increase with the volumetric shrinkage, but decrease when the layer thickness increases. Xu et al. incorporated thermal stresses for shrinkages due to resin phase changes into FEA to simulate the part deformations in SLA [12]. Huang and Lan used a dynamic finite element code to simulate the photopolymerization process so to efficiently select process parameters and to obtain distortion data [13].

We developed a 3D FEA model to simulate the deposition process of FDM by controlling element activations for the involved mechanical and thermal processes [14]. The model can be used to predict residual stresses and evaluate part distortions in FDM. In this study, the developed model was applied to investigate the process parameter effects on the residual stresses and part distortions in FDM.

Numerical Simulations
Commercial software, ANSYS, was utilized to develop the simulation codes. The simulations were conducted in a stepwise thermo-mechanical manner. The element geometry chosen, a rectangular parallelepiped, had dual attributes (Solid45/Solid70), compatible to the thermal and mechanical analyses. The governing equation of the thermal analysis was 3-D transient heat conduction with heat generation from the phase changes. The bottom surface of the model which contacts the platform was set to be constant, chamber temperature (75 $^{\circ}$C). The

boundary conditions of other outer surfaces were forced convection with a heat convection coefficient (86 W/m^2·K) and the chamber temperature. The ABS plastic properties were used. The initial temperature of newly activated elements was set at the extrusion head temperature (280 ^{o}C) and for other activated elements, the initial temperatures carried the result from the previous thermal analysis step. The mechanical analysis was stress equilibrium (elastic structure at the current study) with induced thermal strains. The bottom surface of the part was fully constrained. For newly activated elements, the initial displacement was zero. For other elements, the result of the last mechanical analysis was used as the initial condition. The "element birth/death" function was used to mimic the additive feature in FDM, i.e., continuous filament depositions. The model geometry was first set up, meshed, and the elements were activated according to the filament deposition sequence. For each element activated, a transient thermal analysis started with the current temperature distributions as the initial condition. The calculation continued until the next element was extruded, a function of the element size and the linear deposition speed. The resulted temperature distribution was then used in the next-step mechanical analysis that calculated the displacement at each node of all activated elements. The next element following the designated path was then activated and the convection surface was updated too for the next temperature analysis, and such cycles repeated until all the elements were activated. Displacements, strains, and stresses in the constrained part were analyzed. Then a thermal analysis was executed to change the ambient temperature from the chamber to the laboratory. The displacement constraint of the model was also released in the mechanical analysis to simulate removing the part off the platform.

Parametric Study

The effects of major process parameters in FDM such as the road width, the layer thickness, and the scanning speed were investigated using the developed FEA model. The levels (low, medium, high) of the road width, the layer thickness, and the scan speed tested were 0.25, 0.5, and 1.0 mm, 0.127, 0.254, and 0.508 mm, and 32, 64, 96 mm/s, respectively. The scanning speed varies the heating and cooling frequency during the depositions and will results in different degrees of thermal gradients in the part, affecting residual stresses. The layer thickness and the road width affect the number of the layers and the tool paths required at each layer. A thick layer means less number of layers, which may reduce the number of heating and cooling cycles. On the other hand, a smaller road width will induce less heat into the system within a specific amount of time, but requires more loops to fill a certain area. This will complicate the temperature and stress history and influence the residual stress distributions. Moreover, the effects due to the interactions between the selected parameters are not clearly known.

A second-order approach, Central Composite Design (CCD), was applied in the design of experiments [15]. A typical CCD is made up of 3 portions: the factorial, the central point, and the axial portions. The factorial portion is a 3-factor, 2-level, 1/2 fractional factorial design. Together with 1 center run and 6 axial runs, CCD requires only 15 runs instead of 27 in a 3-factor 3-level full factorial design. Moreover, the CCD method is able to uncover high-order interactions. In this study, the 6 axial runs included either a high or low level of each factor. Due to laborious computational time required for large models, a small part of 40 mm×10 mm×1.016 mm plate, corresponding to the longitudinal, transverse, and height dimensions, was used in the simulations. To discretize the deposition process, a small element, e.g. 1 mm×0.25 mm×0.127 mm, was set as a single unit for activations. In addition, the toolpath used was the long-raster

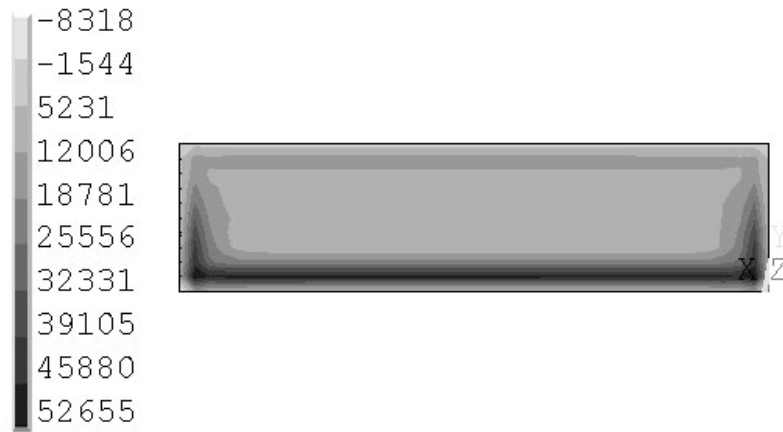pattern, i.e., the primary moving direction of the extrusion head is along with the part longitudinal axis.

Results and Discussion
Simulation Results

Table 1 lists the parameters of each case studied as well as the corresponding simulation result, the maximum first principal stress (σ_1). Figure 1 presents a few examples of first principal stress distributions at different deposition settings (Cases 5, 11, and 4). The stress contours shown are at the part bottom surface where high residual stresses always occur [14]. It can be noted that process parameters have significant effects on the residual stresses in the prototypes. Case 5, corresponding to 1 mm road width, 0.127 mm layer thickness, and 32 mm/s scan speed, results in the lowest residual stresses. Case 11, corresponding to 1 mm road width, 0.254 mm layer thickness and 64 mm/s scan speed, results in an intermediate level of residual stresses. On the other hand, Case 4, corresponding to 0.25 mm road width, 0.508 mm layer thickness, and 96 mm/s scan speed, results in the most severe stress accumulations.

Table 1. The design-of-experiments matrix (-1: low, 0: medium, 1: high) and the simulation results, maximum first principal stress.
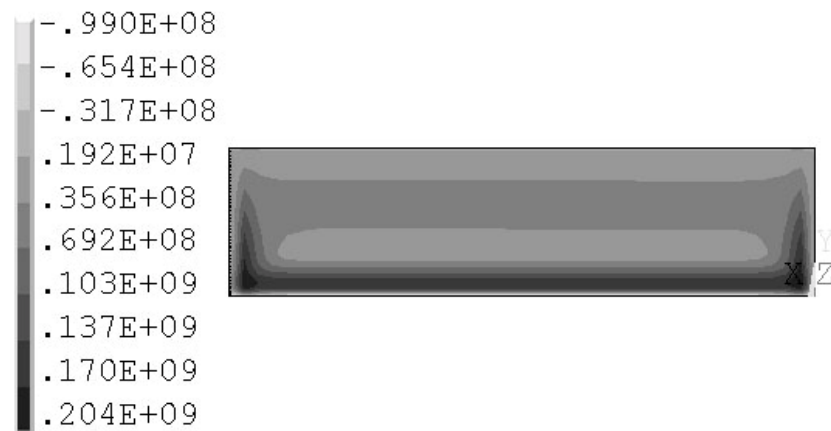
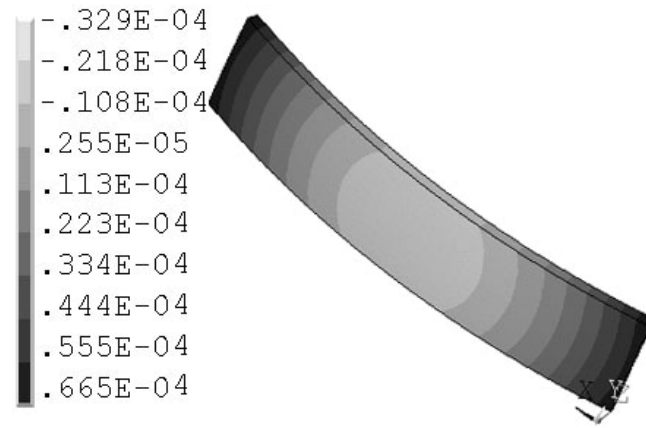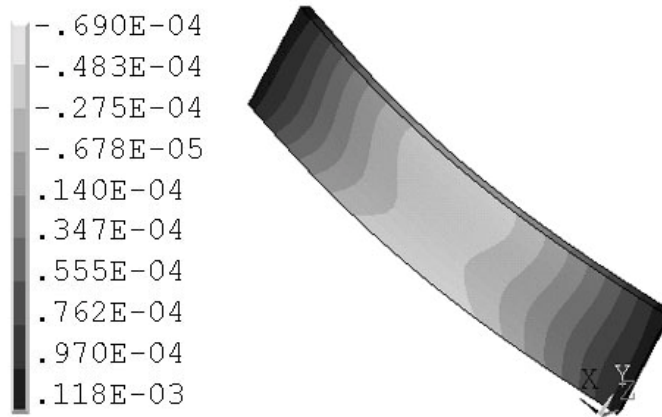| Case #	Factors			Results
	A	B	C	max. σ_1 (kPa)
	Road width	Layer thickness	Scan speed	
1	-1	-1	-1	6.54×10^1
2	-1	-1	1	2.52×10^3
3	-1	1	-1	1.67×10^2
4	-1	1	1	2.04×10^5
5	1	-1	-1	5.27×10^1
6	1	-1	1	8.66×10^4
7	1	1	-1	5.29×10^1
8	1	1	1	6.22×10^4
9	0	0	0	8.31×10^3
10	-1	0	0	2.59×10^2
11	1	0	0	4.59×10^3
12	0	-1	0	1.42×10^2
13	0	1	0	8.33×10^3
14	0	0	-1	7.25×10^1
15	0	0	1	1.06×10^5

(a) Case 5

(b) Case 11

(c) Case 4

Figure 1. First principal stress distribution (σ_1, Pa) at the part bottom surface with different deposition conditions.
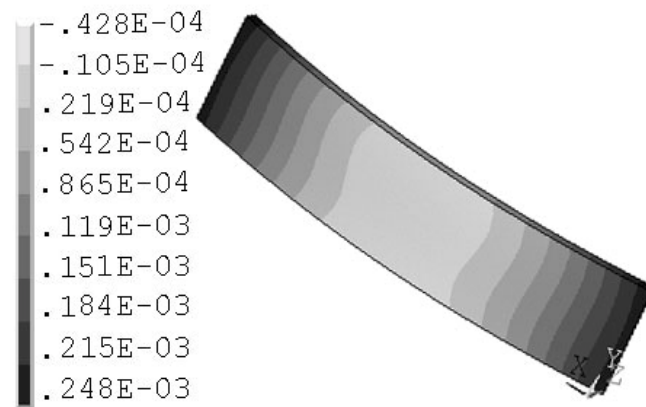
The three cases above were further used to analyze the part distortions after the part was removed off the platform. The simulation results are shown in Figure 2. Figure 3 further plots the part distortion values (flatness) vs. the maximum first principal stress from the three cases. It is shown that the calculated part distortions are correlated with the residual stresses accumulated during the depositions.

(a) Case 5

(b) Case 11

(c) Case 4

Figure 2. Simulated part distortions at different deposition conditions (unit: m).
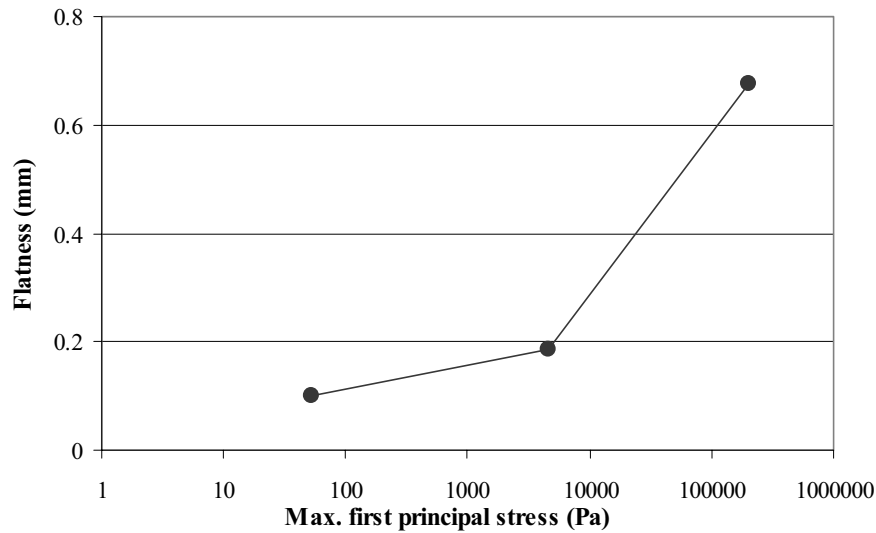
Figure 3. Simulated part flatness vs. the maximum first principal stress in the part.

Statistical Analysis

With the maximum first principle stress (σ_1) as the output variable, the Analysis of Variance (ANOVA) was conducted to identify significant factors and interactions between factors. The results, Table 2 below, show that the scan speed (C) is the most significant factor, followed by the layer thickness (B). The road width (A) alone is insignificant. However, the A-B interaction is considered significant. In addition, there are other high-order interactions, i.e., AB, BC, and ABC that are of secondary significance as well.

Table 2. ANOVA results of maximum first principal stresses.

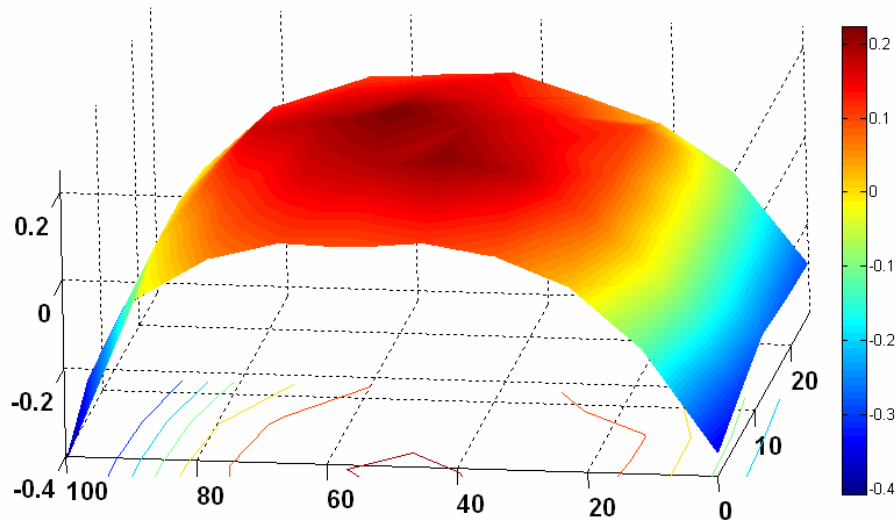| ANOVA of max. σ_1 (kPa)	
Factor	P value
A (road width)	0.2926
B (layer thickness)	0.0138
C (scan speed)	0.0005
AB	0.0046
AC	0.2188
BC	0.0110
ABC	0.0046
AA	0.5779
BB	0.7116
CC	0.0065

After excluding the insignificant interactions, the ANOVA process was performed again, using logarithm values, to reach the prediction equation (1) of maximum σ_1 (in Pa). The regression gives a residue R of 0.94.

$$Log\,(\max.\,\sigma_1) = 6.21 + 0.0676A + 0.494B + 1.31C - 0.432AB$$
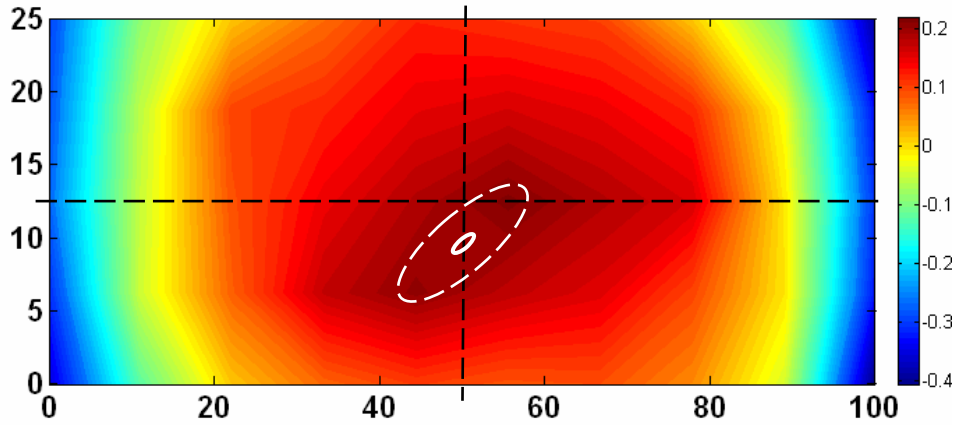$$+ 0.0445BC - 0.0808ABC + 0.168C^2.$$

(1)

Experimental Comparisons

To examine the FEA model, several prototypes were fabricated in an FDM machine and further measured for comparisons. Due to the limitations in accuracy of small part measurements, parts with larger dimensions, but the same length-width ratio were used, 100 mm × 25 mm blocks with a height of 30 mm. In addition to the nominal condition (0.50 mm road width, 0.25 mm layer thickness), two road widths (0.36 and 0.76 mm) and two layer thicknesses (0.18 and 0.33 mm) were varied, giving total 4 sets, to investigate the parameter effects. The fabricated prototypes were removed from the platform and mounted on a metal flat by sealants. The part bottom surface (in reference to deposition) was then probed by a coordinate measuring machine (CMM), automatic measure mode with a total of 50 equally spaced points. The raw data was processed in Matlab to plot the part bottom surface, both 3D height profile and 2D contour plots. The distortion values (flatness) at different parameter settings were compared.

Figure 4 is a typical example of the part bottom surface shape. All measured FDM parts show the same distortion pattern (vaulting shape). However, the flatness value (about 0.63 mm in this example) is not necessarily comparable to the simulation results of small parts. On the other hand, it is noted that the distortion core (the small white-line oval in Figure 4b) shifts away from the part geometric center and the shifting is aligned with the longitudinal axis. Comparing to the simulations (Figure 2), the distortion center shifting is consistent and it is due to the asymmetric stress distribution affected by the toolpath pattern used in the deposition (long-raster in this case). The distortion results at different parameters are compared in Figure 5 (column chart portion) together with the maximum residual stresses (line plot), predicted using Equation (1). It is noted that the distortions increase with both the layer thickness and the road width, however, no discernable effects between these two factors. On the other hand, the simulations indicate that the stress accumulations increase with the layer thickness, and increase with the road width, but to a less extent. At a smaller layer thickness, increasing the road width will elevate the stress accumulations. However, at a larger layer thickness, the road width has little effect on the part residual stresses.

(a) 3D height profile showing the vaulting shape (unit: mm).

(b) 2D contour showing shifting of the distortion center (mm).
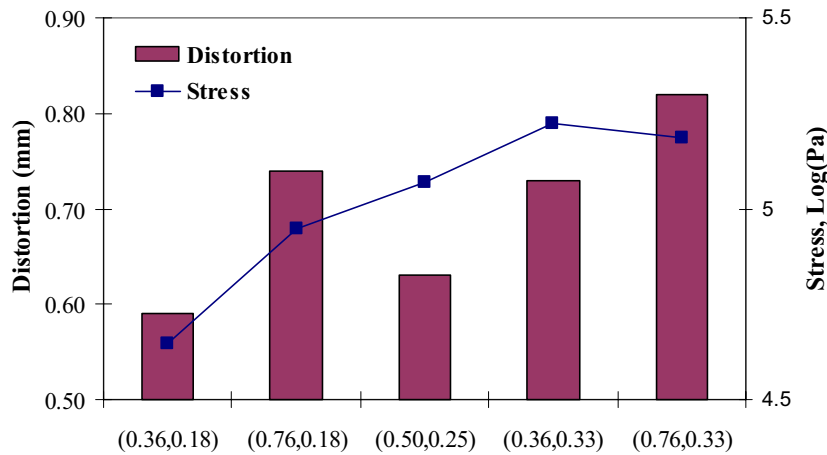Figure 4. An example of part bottom surface distortion.

Figure 5. Part distortion results from the experiment compared with the stress simulations
(variable pair in abscissa is road width and layer thickness, both in mm).

Conclusions

In this study, the FDM process was simulated using a 3D FEA approach incorporating the additive feature and thermomechanical phenomena during the material depositions. The model was tested to evaluate the part distortions, showing vaulting shapes and distortion-core shifting caused by asymmetric stress distributions. The model was employed to study the effects of process parameters on the part distortions in FDM. The design of experiments, using the central composite design scheme, consisted of three factors and three levels. ANOVA was used to identify significant factors and to establish a regression model of the residual stresses. The simulations and analysis can be summarized as follows.

(1) Among the three parameters tested, the scan speed is the most significant factor to the residual stresses followed by the layer thickness.

(2) The road width alone does not affect residual stresses and part distortions in a statistically significant manner. However, the interaction between the road width and the layer thickness seems to be as significant as the layer thickness to part distortions.

(3) There are other two-way and three-way interactions that are of secondary significance.

(4) The simulation results show part distortions are related to the stress accumulation during the depositions.

(5) The simulations indicate that the stress accumulations increase with the increasing layer thickness, also increase with the increasing road width, to a less extent though. The distortion results from the experiment show a similar trend; distortions increase with both the road width and the layer thickness, however, the effects between these two factors are not discernable. A quantitative correlation is yet to be established.

Acknowledgements

References

1. Q. Sun, G.M. Rizvi, V. Giuliani, C.T. Bellehumeur, and P. Gu, "Experimental Study and Modeling of Bond Formation between ABS Filaments in the FDM Process," *Proceedings of Annual Technical Conference - ANTEC*, ANTEC 2004, vol. 1, 2004, pp. 1158-1162.

2. M. Mahesh, Y.S. Wong, Y.H. Fuh, and H.T. Loh, (2004), "Benchmarking for Comparative Evaluation of RP Systems and Processes," *Rapid Prototyping Journal*, vol. 10(2), 2004, pp.123-135.

3. D. Qiu and N.A. Langrana, "Void Eliminating Toolpath for Extrusion-based Multi-material Layered Manufacturing," *Rapid Prototyping Journal*, vol. 8(1), 2002, pp. 38-45.

4. R.C. Pennington, N.L. Hoekstra, and J.L. Newcomer, "Significant Factors on the Dimensional Accuracy of Fused Deposition Modeling," *Proceedings of Annual Technical Conference - ANTEC*, ANTEC 2003, vol. 1, 2003, pp. 880-883.

5. K.Y. Jiang and Y.H. Gu, "Controlling Parameters for Polymer Melting and Extrusion in FDM," *Key Engineering Materials*, vol. 258-259, 2004, pp. 667-671.

6. K.W. Dalgarno, T.H.C. Childs, I. Rowntree, and L. Rothwell, "Finite Element Analysis of Curl Development in the Selective Laser Sintering Process," *Proceedings of Solid Freeform Fabrication Symposium*, University of Texas Austin, 1996, pp.559-566.

7. F.O. Sonmez and T.H. Hahn, "Thermomechanical Analysis of the Laminated Object Manufacturing (LOM) Process," *Rapid Prototyping Journal*, vol. 4(1), 1998, pp. 26-36.

8. R.K. Chin, J.L. Beuth, and C.H. Amon, "Successive Deposition of Metals in Solid Freeform Fabrication Processes, Part 2: Thermomechanical Models of Adjacent Droplets," *Journal of Manufacturing Science and Engineering*, vol. 123, 2001, pp. 632-638.

9. A.H. Nickel, D.M. Barnett, and F.B. Prinz, "Thermal Stresses and Deposition Patterns in Layered Manufacturing," *Materials science and engineering A*, vol. 317, 2001, pp. 59-64.

10. B. Wiedmann, K.H. Dusel, and J. Eschl, "Investigation into Material and Process on Part Distortion," *Rapid Prototyping Journal*, vol. 1(3), 1995, pp. 17-22.

11. G. Bugeda, M. Cervera, G. Lombera, and E. Onate, "Numerical Analysis of Stereolighography Processes Using the Finite Element Method," *Rapid Prototyping Journal*, vol. 1(2), 1995, pp.13-23.

12. H. Xu, Y. Zhang, B. Lu, and D. Chen, "Numerical Simulation of Solidified Deformation of Resin Parts in Stereolithography Rapid Prototyping," *Chinese Journal of Mechanical Engineering*, vol. 40(6), 2004, pp. 107-112.

13. Y.-M. Huang and H.-Y. Lan, "Dynamic Reverse Compensation to Increase the Accuracy of the Rapid prototyping System, *Journal of Materials Processing Technology*, vol. 167(2-3), 2005, pp. 167-176.

14. Y. Zhang and Y.K. Chou, "3D FEA Simulations of Fused Deposition Modeling Process," *Proceedings of MSEC2006*, ASME International Conference on Manufacturing Science and Engineering, October 8-11, 2006, Ypsilanti, MI, in press.

15. S.R. Schmidt and R.G. Launsby, *Understanding Industrial Designed Experiments*, Air Academy Press, Colorado Springs, Colorado, 1997.